

Methods

GeTallele: a mathematical model and a toolbox for integrative analysis and visualization of DNA and RNA allele frequencies

Piotr Słowiński^{1,*}, Muzi Li^{2,#}, Paula Restrepo², Nawaf Alomran², Laim Spurr², Christian Miller², Krasimira Tsaneva-Atanasova¹ and Anelia Horvath^{2,3,4}

¹Department of Mathematics, College of Engineering, Mathematics and Physical Sciences, Living Systems Institute and EPSRC Centre for Predictive Modelling in Healthcare, University of Exeter, EX4 4QJ Exeter, UK, ²McCormick Genomics and Proteomics Center, School of Medicine and Health Sciences, The George Washington University, 20037 Washington, DC, USA, ³Department of Pharmacology and Physiology, School of Medicine and Health Sciences, The George Washington University, 20037 Washington, DC, USA, ⁴Department of Biochemistry and Molecular Medicine, School of Medicine and Health Sciences, The George Washington University, 20037 Washington, DC, USA.

* To whom correspondence should be addressed.

Equal contribution

Associate Editor: XXXXXXXX

Received on XXXXX; revised on XXXXX; accepted on XXXXX

Abstract

Motivation: Asymmetric allele expression typically indicates functional and/or structural features associated with the underlying genetic variants. When integrated, RNA and DNA allele frequencies can reveal patterns characteristic for a wide-range of biological traits, including ploidy changes, genome admixture, allele-specific expression and gene-dosage transcriptional response.

Results: To assess RNA and DNA allele frequencies from matched sequencing datasets, we introduce GeTallele: a toolpack that provides a suit of functions for integrative analysis, statistical assessment and visualization of **Genome** and **Transcriptome allele** frequencies. We demonstrate this functionality across cancer DNA and RNA sequencing sets by detecting novel relationships between encoded and expressed variation that can improve solving of genome composition and expression regulation. In addition, we explore GeTallele as a tool for preliminary assessment of large-scale genomic alterations from RNA-sequencing datasets.

Availability: GeTallele is implemented as a Matlab toolbox available at: <https://git.exeter.ac.uk/pms210/getallele>

Contact: P.M.Slowinski@exeter.ac.uk

Supplementary information: Supplementary data are available at *Bioinformatics* online.

1 Introduction

RNA and DNA carry and present the genetic variation in related, yet distinct, manners; the differences being informative of functional and structural traits. In diploid organisms, an important measure of genetic variation is the allele frequency, which can be measured from both genome (DNA) and transcriptome (RNA) sequencing data (encoded and expressed

allele frequency, respectively). Differential DNA-RNA allele frequencies are associated with a variety of biological processes, such as copy number alterations (CNAs), genome admixture, and allele-specific transcriptional regulation (Ferreira, et al., 2016; Ha, et al., 2012; Han, et al., 2015; Movassagh, et al., 2016; Shah, et al., 2012).

Most of the RNA-DNA allele comparisons from sequencing have been approached at nucleotide level, where it proved to be highly informative for determining the alleles' functionality (Ferreira, et al., 2016; Ha, et al.,

2012; Han, et al., 2015; Macaulay, et al., 2016; Morin, et al., 2013; Movassagh, et al., 2016; Reuter, et al., 2016; Shah, et al., 2012; Shi, et al., 2016; Shlien, et al., 2016; The, et al., 2012; Yang, et al., 2016). Comparatively, integration of allele signals at the molecular level, as derived from linear DNA and RNA carriers, is less explored due to challenges presented by short sequencing length and the related within-molecule (gene or chromosome) heterogeneity of the signal. The different molecular nature of RNA and DNA also leads to limited compatibility of the sequencing output. Herein, we address some of these challenges by employing a mathematical model to assess differences between RNA and DNA of allele frequencies along genes and chromosomes.

2 Methods

2.1 Samples

The GeTallele was developed using sequencing datasets from paired normal and tumour tissue obtained from 72 female patients with breast invasive carcinoma (BRCA) from The Cancer Genome Atlas (TCGA). Each of the 72 datasets contains four matched sequencing datasets: normal exome (Nex), normal transcriptome (Ntr), tumour exome (Tex), and tumour transcriptome (Ttr). In addition, we required each tumour sample to have at least three of the following five purity estimates - Estimate, Absolute, LUMP, IHC, and the consensus purity estimate (CPE), (Supplementary Table 1). Finally, each sample was required to have CNA estimation (genomic segment means based on Genome-Wide-SNPv6 hybridization array) (Aran, et al., 2015; Carter, et al., 2012; Katkovnik, et al., 2002; Pagès, et al., 2010; Yoshihara, et al., 2013; Zheng, et al., 2014).

2.2 Data processing

All the datasets were generated through paired-end sequencing on an Illumina HiSeq platform. The human genome reference (hg38)-aligned sequencing reads (Binary Alignment Maps, .bams) were downloaded from the Genomic Data Commons Data Portal (<https://portal.gdc.cancer.gov/>) and processed downstream through an in-house pipeline. After variant call (Li, 2011), the RNA and DNA alignments, together with the variant lists were processed through the read count module of the package RNA2DNAalign (Movassagh, et al., 2016), to produce variant and reference sequencing read counts for all the variant positions in all four sequencing signals (normal exome, normal transcriptome, tumour exome and tumour transcriptome). Selected read count assessments were visually examined using Integrative Genomics Viewer (Thorvaldsdóttir, et al., 2013).

2.3 Statistics

To test statistical significance, GeTallele uses non-parametric methods and statistical tests (Corder and Foreman, 2014; Hollander, et al., 2013). Namely, to compare distributions of the VAF values we use Kolmogorov-Smirnov test, to compare medians of the variant probability v_{PR} values we use Mann-Whitney-Wilcoxon test, and to study concurrence of windows we use permutation/ bootstrap tests. We use Kendall's tau (Kendall, 1938; Kowalski, 1972; Newson, 2002) to analyse correlations between v_{PR} and admixture purity measures. We use Kendall's tau (Kendall, 1938; Kowalski, 1972; Newson, 2002) to analyse correlations between v_{PR} and admixture purity measures.

To test relations between v_{PR} and CNA we use Pearson's correlation coefficients tested against 10000 permutations of the data. We use Pearson's correlation coefficient (rather than Spearman's or Kendall's) because we expect the relation to be linear and we consider the high values of v_{PR} and CNA to be important and informative for the analysis. We use a permutation test to quantify the statistical significance because the v_{PR} and CNA values do not have normal distributions, and hence the analytical expression of the significance of the Pearson's correlation is invalid.

To account for multiple comparisons between VAF distributions in the windows we set the probability for rejecting the null hypothesis at $p < 1e-5$, which corresponds to Bonferroni (Dunn, 1961) family-wise error rate (FWER) correction against 5000 comparisons. We use a fixed value, rather than other approaches, to ensure better consistency and reproducibility of the results. When appropriate, we also apply Benjamini and Hochberg (Benjamini and Hochberg, 1995) false discovery rates (FDR) correction with a probability of accepting false positive results $p_{FDR} < 0.1$.

3 Results

GeTallele mathematically and statistically compares RNA and DNA variant allele frequencies (VAF_{RNA} and VAF_{DNA}) at positions of interest, and visualizes the allele distribution at desired resolution from nucleotide to genome (Figure 1). VAFs are estimated from sequencing data and are based on the counts of the variant and reference reads (n_{VAR} and n_{REF}) covering each position of interest in a dataset: $VAF = n_{VAR} / (n_{VAR} + n_{REF})$. Analysis of the VAF_{RNA} and VAF_{DNA} in the GeTallele is based on comparing probability of observing a given VAF value at various positions of interest. Estimation of the variant allele probability, v_{PR} , is implemented using a mathematical model of distribution of the VAF values and is the core functionality of the GeTallele (See section 3.1 for details of the model). We demonstrate the GeTallele functionality using matched normal and tumour DNA and RNA sequencing data (i.e. four sequencing signals per sample: normal exome, normal transcriptome, tumour exome and tumour transcriptome); for each sample, the set of variant loci is determined based on the heterozygote calls in the normal exome (Li, et al., 2009).

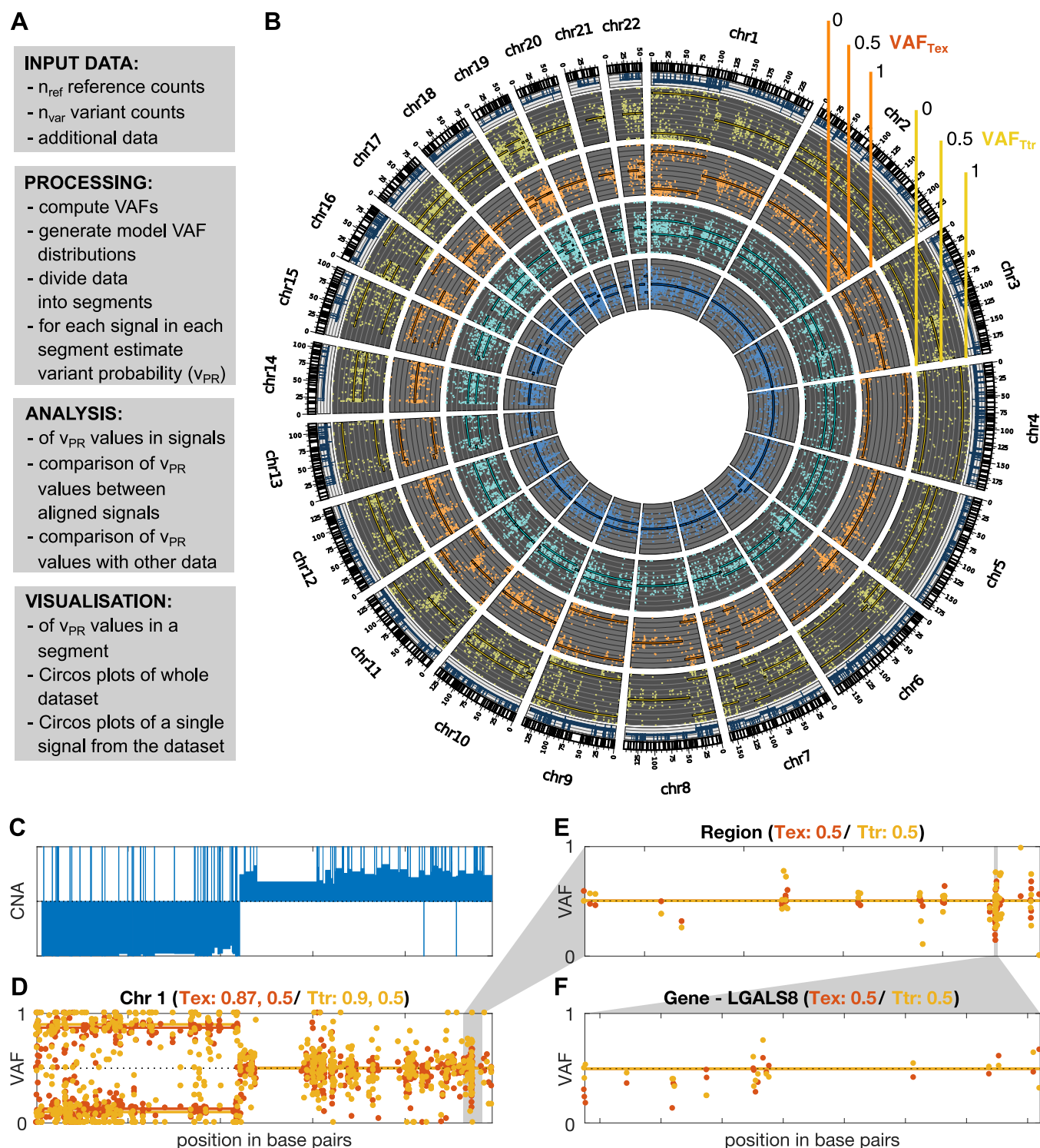


Fig. 1. GeTallele and visualisation of VAF data. **A** Toolbox description. **B** Visualisation of the whole dataset on the level of genome using Circos plot (blue – normal exome, cyan – normal transcriptome, orange – tumour exome, yellow – tumour transcriptome). **C - F** show in details VAF_{Tex} and VAF_{Ttr} values of chromosome 1; **C - F** Visualization of the VAF values with fitted variant probability (v_{PR} – see Section 3.1 and Figure 2) values at the level of chromosome (**D**), custom genome region (**E**) and gene (**F**), for the chromosome level shown also are CNA values (**C**). Panel **D** shows that there are two segments with different VAF distributions. Panel **C** shows that change in the CNA is concurrent with the change in the VAF distributions. Tex - tumour exome (orange); Ttr - tumour transcriptome (yellow).

3.1 Model for estimation of variant probability v_{pr}

3.1.1 Data segmentation

To analyse VAF at genome-wide level, GeTallele first divides the VAF dataset into a set of non-overlapping windows along the chromosomes. Segmentation of the dataset into windows is based on a sequencing signal chosen out of all the available datasets in the aggregated aligned VAF dataset (one out of four in the presented analysis). Each window contains all the sequencing signals that are in the analysed dataset.

To partition the data into the windows GeTallele uses a parametric global method, which detects the breakpoints in the signals using its mean, as implemented in the Matlab function `findchangepts` (Killick, et al., 2012; Lavielle, 2005). In each window, the VAF values of the chosen signal have a mean that is different from the mean in the adjacent windows. Sensitivity of breakpoint detection can be controlled using parameter `MinThreshold`, in the presented analysis it was set to 0.2. For segmentation and analysis (without loss of generality) we transform all the original VAF values to $VAF = |VAF - 0.5| + 0.5$.

3.1.2 Variant probability

In each window, separately for each sequencing signal, GeTallele estimates variant probability, v_{pr} - probability of observing a variant allele. The v_{pr} is a parameter that describes the genomic event that through the sequencing process was transformed into a specific distribution of VAF values found in the signal. For example, in VAF_{DNA} from a diploid genome, variant probability $v_{pr}=0.5$ (meaning that both alleles are equally probable) corresponds to a true allelic ratio of 1:1 for heterozygote sites. For heterozygote sites in the normal DNA, the corresponding tumour VAF_{DNA} is expected to have the following interpretations: $v_{pr}=1$ or $v_{pr}=0$ corresponds to a monoallelic status resulting from a deletion, and $v_{pr}=0.8$, 0.75, 0.67 correspond to allele-specific tetra-, tri-, and duplication of the variant-bearing allele, respectively.

The v_{pr} of the VAF_{RNA} is interpreted as follows. In positions corresponding to DNA heterozygote sites, alleles not preferentially targeted by regulatory traits are expected to have expression rates with variant probability $v_{pr}=0.5$, which (by default) scale with the DNA allele distribution. Differences between VAF_{DNA} and VAF_{RNA} values are observed in special cases of transcriptional regulation where one of the alleles is preferentially transcribed over the other. In the absence of allele-preferential transcription, VAF_{DNA} and VAF_{RNA} are anticipated to have similar v_{pr} across both diploid (normal) and aneuploid (affected by CNAs) genomic regions. Consequently, VAF_{DNA} and VAF_{RNA} are expected to synchronously switch between allelic patterns along the chromosomes, with the switches indicating break points of DNA deletions or amplifications.

To estimate v_{pr} in the signals, GeTallele first generates model VAF distributions and then uses the earth mover's distance (EMD) (Kantorovich and Rubinstein, 1958; Levina and Bickel, 2001) to fit them to the data. To generate a model VAF distribution that correspond to a genomic event with a given variant probability, v_{pr} , GeTallele, bootstraps 10000 values of the total reads (sum of the variant and reference reads; $n_{VAR} + n_{REF}$) from the analysed signal in dataset. It then uses binomial pseudorandom number generator to get number of successes for given number of total reads and a given value of v_{pr} (implemented in the Matlab function `binornd`). The v_{pr} is the probability of success and generated number successes is interpreted as an n_{VAR} .

Since we observed that DNA and RNA signals have different distributions of total reads, GeTallele generates the model VAF distributions separately for each of the four sequencing signals in the datasets. GeTallele generates the models separately for each dataset because the distributions

of total reads vary between participants. Analysis presented in the paper uses 51 model VAF distributions with v_{pr} values that vary from 0.5 to 1 with step 0.01. The model VAF distributions are parametrized using only $v_{pr} \geq 0.5$, however to generate them we use v_{pr} and its symmetric counterpart $1 - v_{pr}$. Examples of model VAF distributions with different values of v_{pr} are shown in Figure 2.

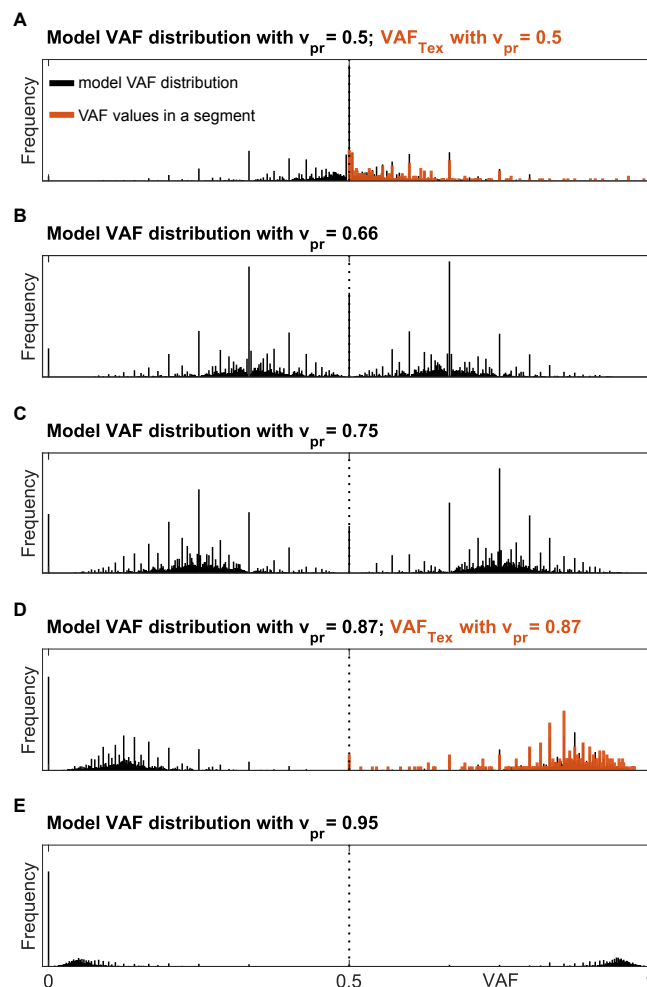


Fig. 2. Model and real VAF distributions. A - E Model VAF distributions for different values of v_{pr} . Panels A and D show additionally distributions of VAF_{TEX} for the two windows shown in Figure 1D.

3.1.3 Earth mover's distance

EMD is a mathematical metric for quantifying differences between probability distributions (Kantorovich and Rubinstein, 1958; Levina and Bickel, 2001) and for univariate distributions can be computed as

$$EMD(PDF_1, PDF_2) = \int_Z |CDF_1(z) - CDF_2(z)| dz.$$

Here, PDF_1 and PDF_2 are two probability density functions and CDF_1 and CDF_2 are their respective cumulative distribution functions. Z is the support of the PDFs (i.e. set of all the possible values of the random variables described by them). Because VAFs are defined as simple fractions with values between 0 and 1, their support is given by a Farey sequence (Hardy,

GeTallele toolbox

et al., 2008) of order n ; n is the highest denominator in the sequence. For example Farey sequence of order 2 is 0, 1/2, 1 and Farey sequence of order 3 is 0, 1/3, 1/2, 2/3, 1. GeTallele uses a Farey sequence of order 1000 for all the EMD computations.

To estimate v_{PR} , GeTallele computes EMD between the distribution of the VAF values of each signal in the window and the 51 model VAF distributions (i.e. observed vs modelled VAF), the estimate is given by the v_{PR} of the model VAF distribution that is closest to the VAF distribution in the window. Examples of VAF distributions with fitted model VAF distributions are shown in Figure 2A and D. Dependence of the confidence intervals of the estimation on the number of VAF values in a window is presented in Figure 3.

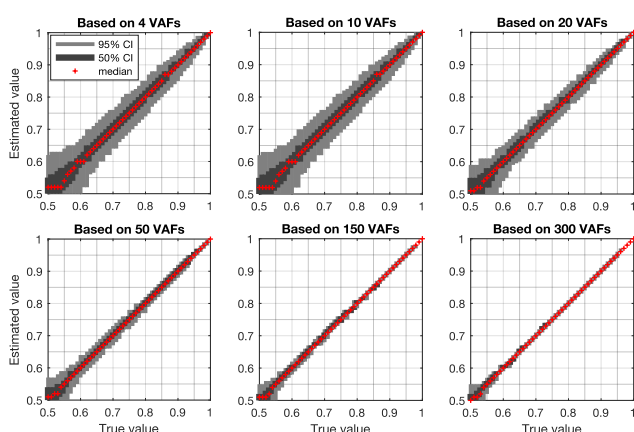


Fig. 3. Confidence intervals for samples with different numbers of VAFs. Each confidence interval is based on estimation of v_{PR} in 1000 randomly generated samples with set v_{PR} (True value). Light grey bar is 95% confidence interval (950 samples lay within this interval), dark grey bar is 50% confidence interval (500 samples lay within this interval), red cross is median value.

3.2 Analysis

GeTallele is readily applicable to assess RNA-DNA relationships between normal and tumour sequencing signals derived from the same sample/individual (matched datasets). As a proof of concept, we assessed matched normal and tumour exome and transcriptome sequencing data of 72 breast carcinoma (BRCA) datasets with pre-assessed copy-number and genome admixture estimation acquired through TCGA (Supplementary Table 1). For these datasets, purity and genome admixture has been assessed using at least three of the following five approaches: ESTIMATE, ABSOLUTE, LUMP, IHC, and the Consensus Purity Estimation (CPE) (Aran, et al., 2015; Carter, et al., 2012; Katkovnik, et al., 2002; Pagès, et al., 2010; Yoshihara, et al., 2013; Zheng, et al., 2014). In addition, on the same datasets we applied THetA – a popular tool for assessing CNA and admixture from sequencing data (Oesper, et al., 2013; Oesper, et al., 2014).

3.2.1 Segmentation results

Segmentation of the data, based on the tumour exome signal, resulted in 2699 windows across the 72 datasets. We excluded from further analysis 289 windows where either tumour exome or transcriptome had $v_{PR} \geq 0.58$ but their VAF distribution could not be differentiated from the model VAF distributions with $v_{PR} = 0.5$ ($p > 1e-5$, Kolmogorov Smirnov test, equivalent to Bonferroni FWER correction for 5000 comparisons). The 289 excluded windows correspond to 4% of the data in terms of number of base pairs in

the windows and 4% of all the available data points; i.e. they are short and contain only few VAF values. In the remaining 2410 windows, we systematically examined the similarity between corresponding $v_{AF_{TEX}}$ (tumour exome), $v_{AF_{TTR}}$ (tumour transcriptome) and CNA. We documented several distinct patterns of coordinated RNA-DNA allelic behaviour as well as correlations with CNA data.

In 65% of all analysed windows the distributions of $v_{AF_{TEX}}$ and $v_{AF_{TTR}}$ were concordant (had the same v_{PR} and $p > 1e-5$, Kolmogorov Smirnov test), and in 35% they were discordant ($p < 1e-5$, Kolmogorov Smirnov test). In 1% of all windows $v_{AF_{TEX}}$ and $v_{AF_{TTR}}$ had the same v_{PR} but had statistically different distributions ($p < 1e-5$, Kolmogorov Smirnov test), we consider such windows as concordant; Kolmogorov-Smirnov test is very sensitive for differences between distributions, v_{PR} fitting is more robust. In the vast majority of the discordant windows v_{PR} of the $v_{AF_{TTR}}$, $v_{PR_{TTR}}$, was higher than v_{PR} of the $v_{AF_{TEX}}$, $v_{PR_{TEX}}$, (only in 21 out of 944 windows $v_{PR_{TTR}}$ was lower than $v_{PR_{TEX}}$).

3.2.2 Correlation with purity

In windows with discordant $v_{AF_{TEX}}$ and $v_{AF_{TTR}}$ distributions, we observed significant negative correlation between the difference ($v_{PR_{TTR}} - v_{PR_{TEX}}$) and the samples' purity estimates (ESTIMATE: $\tau = -0.16$, $p = 0.0005$; ABSOLUTE: $\tau = -0.33$, $p = 1.2e-13$; LUMP: $\tau = -0.6$, $p = 9.3e-29$; IHC: $\tau = -0.13$, $p = 0.003$; CPE: $\tau = -0.3$, $p = 5.5e-11$, Kendall's tau; see also Figure 4).

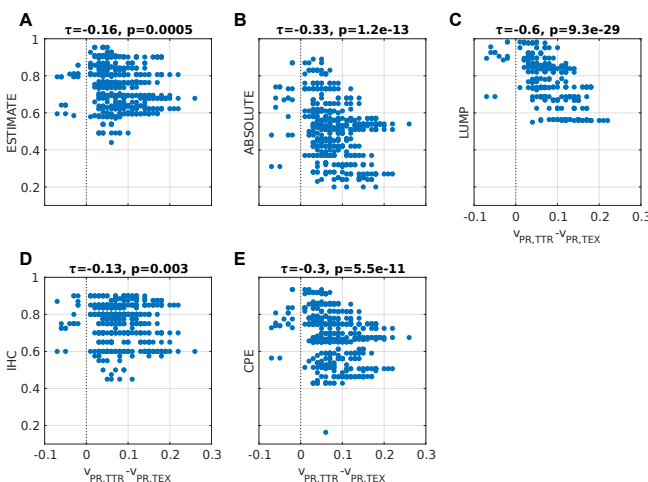


Fig. 4. Illustration of correlations between estimates of sample purity and $v_{PR_{TTR}} - v_{PR_{TEX}}$ in windows where $v_{AF_{TEX}}$ and $v_{AF_{TTR}}$ are statistically discordant ($p < 1e-5$, Kolmogorov Smirnov test).

3.2.3 Concurrence of segmentation based on DNA and RNA

We next analysed the concurrence between windows resulting from independent segmentations of the dataset based on the tumour exome and transcriptome signals in the datasets (2699 and 3603 windows, respectively, across all the samples). We first assessed chromosome-wise alignment of the start and end points of the windows. In 45% of the chromosomes both $v_{AF_{TEX}}$ and $v_{AF_{TTR}}$ signals produce a single window that contains the whole chromosome. In 33% of chromosomes both signals produced multiple windows. These windows are well aligned, with 90% of the break points within 7% difference in terms of number of data points in the chromosome (Q50=0.02%, Q75=2% of data points in the chromosome). Probability of observing such an alignment by chance is smaller than $p = 1e-5$

(100,000 bootstrap samples with breaking points assigned randomly in all the individual chromosomes where both signals produced multiple windows). In 22% of the chromosome windows based on VAF_{TEX} and VAF_{TTR} signals were positionally discordant – one signal produced a single window containing whole chromosome while the other produced multiple windows.

To compare the v_{PR} values in the 55% of chromosomes where at least one signal produced single window, we computed chromosome-wise mean absolute error (MEA) between the v_{PR} in two sets of windows. To account for different start and end points of the windows we interpolated the v_{PR} values (nearest neighbour interpolation) at each data point in the chromosome. We separately compared the $v_{PR,TEX}$ and $v_{PR,TTR}$ values. The alignment in terms of MEA is very good, $v_{PR,TEX}$ agreed perfectly in 8% of the chromosomes and had the percentiles of MEA equal to Q50=0.013, Q75=0.02 and Q97.5=0.05, while $v_{PR,TTR}$ also agreed perfectly in 8% but had slightly higher percentiles of MEA Q50=0.02, Q75=0.033 and Q97.5=0.068. $v_{PR,TEX}$ and $v_{PR,TTR}$ values had MEA=0 simultaneously in 4% of the chromosomes. Probability of observing such values of MEA by chance is smaller than $p=1e-3$ (1000 random assignments of $v_{PR,TEX}$ and $v_{PR,TTR}$ values to windows in the 873 chromosomes where at least one signal had more than one window). It is noteworthy that MEA Q97.5<0.07 is comparable with the confidence interval of single v_{PR} estimate; compare Figure 3. In other words, both signals in a sample (Tex and Ttr) give very similar results in terms of windows' segmentation and estimated values of the v_{PR} . Albeit, segmentation of VAF_{TTR} generates higher number of windows. Figure 5 shows examples of concurrence between windows based on VAF_{TEX} and VAF_{TTR} signals in a positionally concordant chromosome (both signals produced multiple windows).

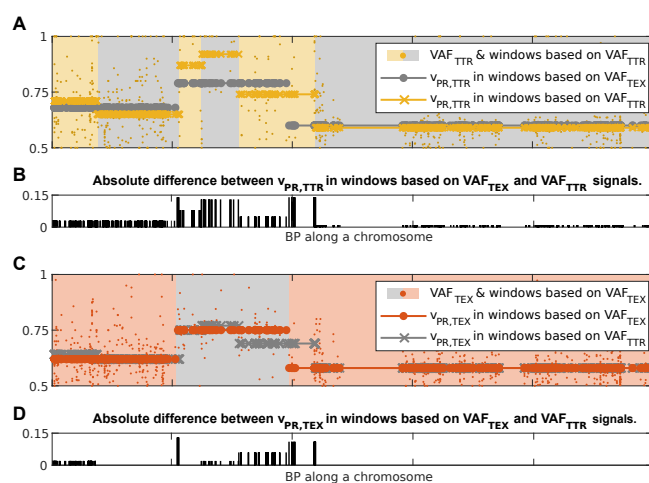


Fig. 5. Illustration of concurrence between windows resulting from independent segmentations of the dataset based on the VAF_{TEX} and VAF_{TTR} signals. A yellow dots, VAF_{TTR}; grey circles, $v_{PR,TTR}$ interpolated at all data points in windows based on VAF_{TEX}; yellow crosses, $v_{PR,TTR}$ interpolated at all data points in windows based on VAF_{TTR}. B bar plot of the absolute difference between the v_{PR} values in the two kinds of windows. C orange dots, VAF_{TEX}; grey crosses, $v_{PR,TEX}$ interpolated at all data points in windows based on VAF_{TEX}; orange dots $v_{PR,TEX}$ interpolated at all data points in windows based on VAF_{TTR}. D bar plot of the absolute difference between the v_{PR} values in the two kinds of windows.

3.2.4 Correlation between v_{PR} and CNA

Finally, we analysed the correlations between v_{PR} and CNA in the individual datasets. We separately computed correlations for deletions and amplifications. In order to separate deletions and amplifications, for each data set we found CNA_{MIN} , value of the CNA in the range -0.25 to 0.25 that had the smallest corresponding $v_{PR,TEX}$. To account for observed variability of the CNA values near the CNA_{MIN} , we set the threshold for amplifications to $CNA_A = CNA_{MIN} - 0.05$, and for deletions we set it to $CNA_D = CNA_{MIN} + 0.05$. For VAF_{TEX} we observed significant correlations with negative trend between $v_{PR,TEX}$ and $CNA \leq CNA_D$ in 58 datasets and with positive trend between $v_{PR,TEX}$ and $CNA \geq CNA_A$ in 39 datasets ($p_{FDR} < 0.05$, Pearson's correlation with Benjamini Hochberg FDR correction). For VAF_{TTR} we observed significant correlations with negative trend between $v_{PR,TTR}$ and $CNA \leq CNA_D$ in 65 datasets and with positive trend between $v_{PR,TTR}$ and $CNA \geq CNA_A$ in 32 datasets ($p_{FDR} < 0.05$, Pearson correlation with Benjamini Hochberg correction). Such strong correlations indicate that v_{PR} accurately captures information contained in CNA. Although, it does not differentiate between positive and negative values of the CNA.

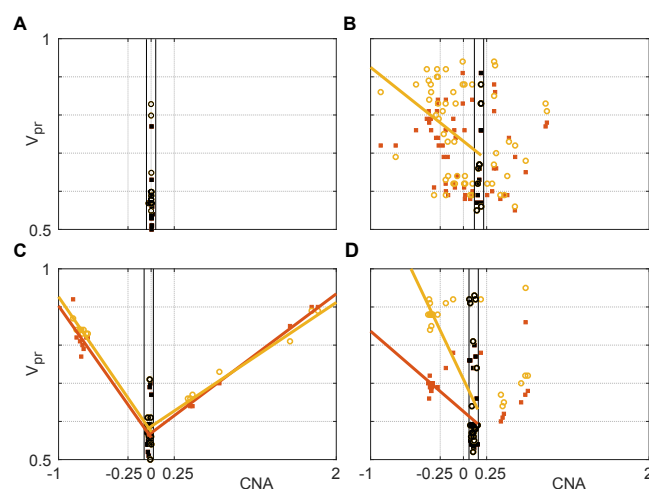


Fig. 6. Illustration of the correlations between v_{PR} and CNA. Orange squares $v_{PR,TEX}$, yellow circles $v_{PR,TTR}$. Lines, least-squares fitted trends for significant correlations (orange correlation with $v_{PR,TEX}$, yellow correlation with $v_{PR,TTR}$). Black, v_{PR} for $CNA_{MIN} \pm 0.05$. Correlations for all the datasets are shown in Supplementary Figure 1. A there are no significant correlations, all the values of CNA are close to $CNA_{MIN}=0$. B relationship between CNA and v_{PR} is noisy, only some correlations are statistically significant. C all the correlations are statistically significant, $v_{PR,TTR}$ values (circles) follow closely the $v_{PR,TEX}$ (squares) indicating that in most of the windows distributions of the VAF_{TEX} and VAF_{TTR} are concordant. D only correlations for $CNA \leq CNA_D$ are statistically significant.

Figure 6 shows four typical patterns of correlation between the CNA and v_{PR} values observed in the data. In Figure 6A there are no significant correlations, all the values of CNA are close to CNA_{MIN} . In Figure 6B relationship between CNA and v_{PR} is noisy, only correlation between $v_{PR,TTR}$ and $CNA \leq CNA_D$ are statistically significant. In Figure 6C all the correlations are statistically significant, $v_{PR,TTR}$ values (circles) follow closely the $v_{PR,TEX}$ (squares) indicating that in most of the windows distributions of the VAF_{TEX} and VAF_{TTR} are concordant. In Figure 6D correlations between $v_{PR,TEX}$, $v_{PR,TTR}$ and $CNA \leq CNA_D$ are statistically significant, but there is big difference (with median of 0.18) between $v_{PR,TEX}$ and $v_{PR,TTR}$ values, indicating that in most of the windows the distributions of the VAF_{TEX} and VAF_{TTR} in this dataset are discordant. Visual inspection of the data reveals that for many datasets the correlations are visible, but

GeTallele toolbox

they do not reach statistical significance due to small number of points or strong outliers. This further, indicates that v_{PR} and CNA measures are concordant in terms of information that they contain.

4 Discussion

Integrative analysis of RNA and DNA sequence data is facilitated by the growing availability of RNA and DNA sequencing datasets and by the technological advances now enabling simultaneous RNA and DNA sequencing from the same source (Macaulay, et al., 2016; Reuter, et al., 2016; The, et al., 2012). However, RNA and DNA integrative analyses are challenged by limited compatibility between RNA and DNA datasets and high technical variance of the sequencing-produced signals. Our approach – GeTallele – addresses the compatibility restricting the analyses within confidently co-covered DNA and RNA regions, and the high variability - through computing the distance between the two distributions.

Using GeTallele, we detected several intriguing relationships between DNA-RNA allele frequencies and biological processes. First, in chromosomes affected by deletions and amplifications, VA_{RNA} and VA_{DNA} showed highly concordant break point calls. This indicates that VA_{RNA} alone can serve as preliminary indicator for deletions and amplifications, which can facilitate the applications of RNA-sequencing analysis on the large and constantly growing collections of transcriptome sequencing data. Second, higher difference between VA_{TTR} and VA_{TEX} distributions ($v_{PR,TTR} - v_{PR,TEX}$), indicative for higher level of allele-specific expression, correlated with low sample purity (see Figure 4). Biologically, this observation likely implicates higher level of imprinting (transcription from one of the DNA alleles) in samples with low genome integrity, which is generally aligned with the increased number of CNAs and the fast replication cycle in advances tumour samples.

Based on our results, variant probability v_{PR} can serve as a dependable indicator to assess gene and chromosomal allele asymmetries and to aid calls of genomic events. Importantly, GeTallele allows to visualize the observed patterns, with the ability to magnify regions of interest to desired resolution, including chromosome, gene, or custom genome region, along with statistical measures of the modes, for all the modes in the examined segment.

Acknowledgements

Funding

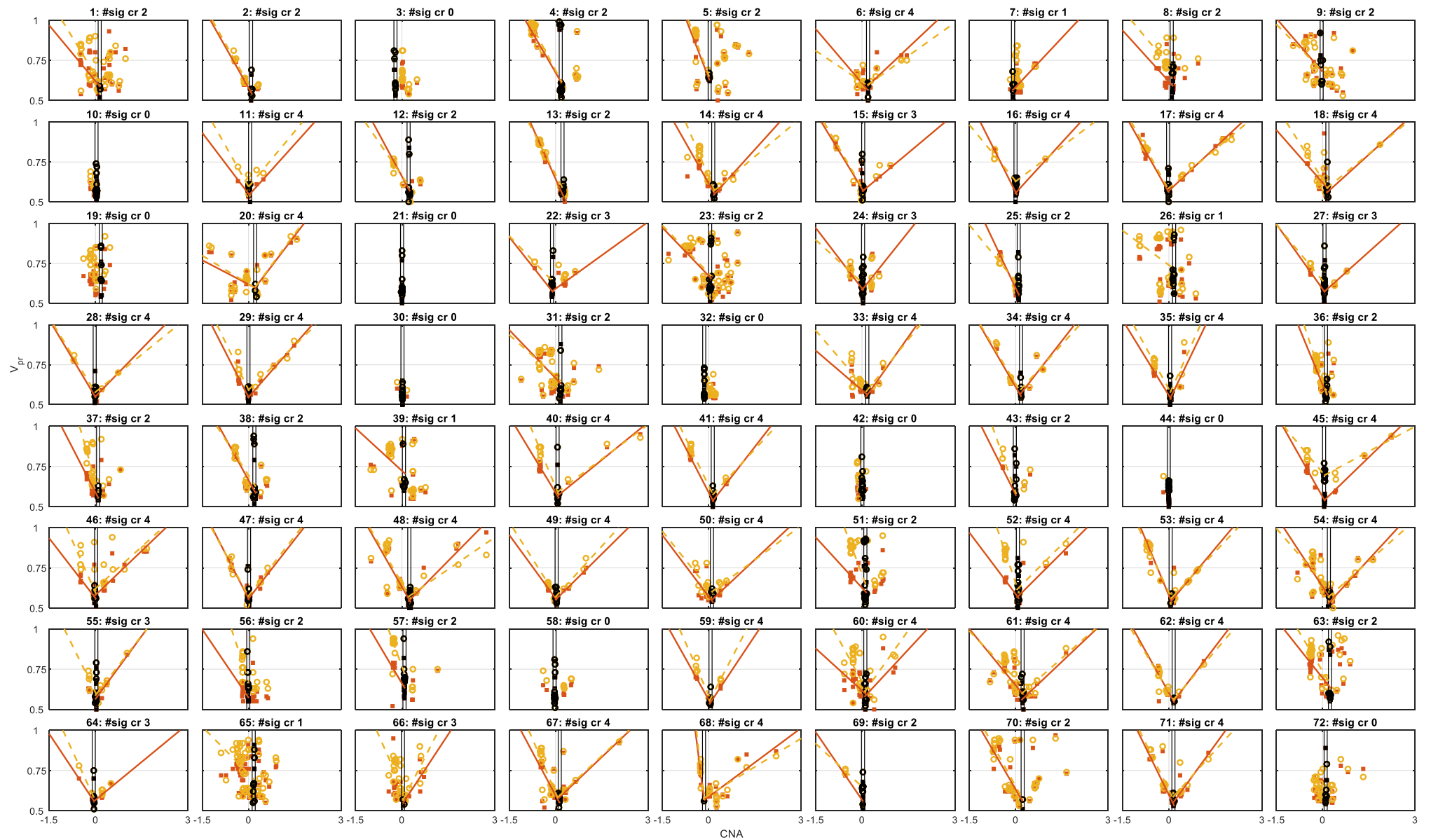
This work was supported by McCormick Genomic and Proteomic Center (MGPC), The George Washington University; [MGPC_PG2018 to A.H.]. Work of P.S. was generously supported by the Wellcome Trust Institutional Strategic Support Award [204909/Z/16/Z].

Conflict of Interest: none declared.

References

Aran, D., Sirota, M. and Butte, A.J. Systematic pan-cancer analysis of tumour purity. *Nature communications* 2015;6:8971.
 Benjamini, Y. and Hochberg, Y. Controlling the False Discovery Rate - a Practical and Powerful Approach to Multiple Testing. *J Roy Stat Soc B Met* 1995;57(1):289-300.
 Carter, S.L., et al. Absolute quantification of somatic DNA alterations in human cancer. *Nature biotechnology* 2012;30(5):413-421.
 Corder, G.W. and Foreman, D.I. *Nonparametric Statistics*. John Wiley & Sons; 2014.
 Dunn, O.J. Multiple Comparisons among Means. *J Am Stat Assoc* 1961;56(293):52-64.

Ferreira, E., Shaw, D.M. and Oddo, S. Identification of learning-induced changes in protein networks in the hippocampi of a mouse model of Alzheimer's disease. *Translational psychiatry* 2016;6(7):e849.
 Ha, G., et al. Integrative analysis of genome-wide loss of heterozygosity and mono-allelic expression at nucleotide resolution reveals disrupted pathways in triple-negative breast cancer. *Genome research* 2012;22(10):1995-2007.
 Han, L., et al. Alternative applications for distinct RNA sequencing strategies. *Briefings in bioinformatics* 2015;16(4):629-639.
 Hardy, G.H., et al. *An introduction to the theory of numbers*. Oxford ; New York: Oxford University Press; 2008.
 Hollander, M., Wolfe, D.A. and Chicken, E. *Nonparametric Statistical Methods*. John Wiley & Sons; 2013.
 Kantorovich, L.V. and Rubinstein, G.S. On a space of completely additive functions. *Vestnik Leningrad. Univ* 1958;13(7):52-59.
 Katkovnik, V., Kgiarzian, K. and Astola, J. Adaptive window size image de-noising based on intersection of confidence intervals (ICI) rule. *J Math Imaging Vis* 2002;16(3):223-235.
 Kendall, M.G. A new measure of rank correlation. *Biometrika* 1938;30(1-2):81-93.
 Killick, R., Fearnhead, P. and Eckley, I.A. Optimal Detection of Change-points With a Linear Computational Cost. *J Am Stat Assoc* 2012;107(500):1590-1598.
 Kowalski, C.J. On the Effects of Non-Normality on the Distribution of the Sample Product-Moment Correlation Coefficient. *Journal of the Royal Statistical Society. Series C (Applied Statistics)* 1972;21(1):1-12.
 Lavielle, M. Using penalized contrasts for the change-point problem. *Signal Process* 2005;85(8):1501-1510.
 Levina, E. and Bickel, P. The Earth Mover's distance is the Mallows distance: some insights from statistics. In, *IEEE International Conference on Computer Vision* 2001. p. 251-256.
 Li, H. A statistical framework for SNP calling, mutation discovery, association mapping and population genetical parameter estimation from sequencing data. *Bioinformatics* 2011;27(21):2987-2993.
 Li, H., et al. The Sequence Alignment/Map format and SAMtools. *Bioinformatics* 2009;25(16):2078-2079.
 Macaulay, I.C., et al. Separation and parallel sequencing of the genomes and transcriptomes of single cells using G&T-seq. *Nature protocols* 2016;11(11):2081-2103.
 Morin, R.D., et al. Mutational and structural analysis of diffuse large B-cell lymphoma using whole-genome sequencing. *Blood* 2013;122(7):1256-1265.
 Movassagh, M., et al. RNA2DNAalign: nucleotide resolution allele asymmetries through quantitative assessment of RNA and DNA paired sequencing data. *Nucleic acids research* 2016;44(22):e161.
 Newson, R. Parameters behind "nonparametric" statistics: Kendall's tau, Somers' D and median differences. *Stata Journal* 2002;2(1):45-64.
 Oesper, L., Mahmoody, A. and Raphael, B.J. THetA: inferring intra-tumor heterogeneity from high-throughput DNA sequencing data. *Genome biology* 2013;14(7):R80.
 Oesper, L., Satas, G. and Raphael, B.J. Quantifying tumor heterogeneity in whole-genome and whole-exome sequencing data. *Bioinformatics (Oxford, England)* 2014;30(24):3532-3540.
 Pagès, F., et al. Immune infiltration in human tumors: a prognostic factor that should not be ignored. *Oncogene* 2010;29(8):1093-1102.
 Reuter, J.A., et al. Simul-seq: combined DNA and RNA sequencing for whole-genome and transcriptome profiling. *Nature methods* 2016;13(11):953-958.
 Shah, S.P., et al. The clonal and mutational evolution spectrum of primary triple-negative breast cancers. *Nature* 2012;486(7403):395-399.
 Shi, L., et al. Long-read sequencing and de novo assembly of a Chinese genome. *Nature communications* 2016;7:12065.
 Shlien, A., et al. Direct Transcriptional Consequences of Somatic Mutation in Breast Cancer. *Cell reports* 2016;16(7):2032-2046.
 The, E.P.C., et al. An integrated encyclopedia of DNA elements in the human genome. *Nature* 2012;489:57.
 Thorvaldsdóttir, H., Robinson, J.T. and Mesirov, J.P. Integrative Genomics Viewer (IGV): high-performance genomics data visualization and exploration. *Briefings in bioinformatics* 2013;14(2):178-192.
 Yang, S., et al. An Integrated Approach for RNA-seq Data Normalization. *Cancer informatics* 2016;15:129-141.
 Yoshihara, K., et al. Inferring tumour purity and stromal and immune cell admixture from expression data. *Nature communications* 2013;4:2612.
 Zheng, X., et al. MethylPurify: tumor purity deconvolution and differential methylation detection from single tumor DNA methylomes. *Genome biology* 2014;15(8):419.



Supplementary Fig. 1. Illustration of the correlations between v_{pr} and CNA. Orange squares $v_{pr,TEX}$, yellow circles $v_{pr,TTR}$. Lines, least-squares fitted trends for significant correlations (orange correlation with $v_{pr,TEX}$, yellow correlation with $v_{pr,TTR}$). Black, v_{pr} for $CNA_{MIN} \geq 0.05$. Title format Number of the dataset: #sig cr number of significant correlations in the dataset.

Supplementary Table 1. Datasets, signals and purity estimates.

#	TCGA BRCA datasets	EST	ABS	LUMP	IHC	CPE
1	001_Nex_BRCA_TCGA-BH-A1FC-11A_413b80f6-f6cf-4992-804a-f045e38cbe6f 001_Ntr_BRCA_TCGA-BH-A1FC-11A_086db136-f3f2-42fa-aca1-63847de6ccb9 001_Tex_BRCA_TCGA-BH-A1FC-01A_1a2187a6-aea8-4096-8c3f-208a8467cd5a 001_Ttr_BRCA_TCGA-BH-A1FC-01A_b5e2f568-e6fc-4192-a3ab-da956e5bfa4c	0.7615	0.49	0.6693	0.9	0.6517
2	002_Nex_BRCA_TCGA-BH-A0B5-11A_c724807c-d80d-4582-8238-8339397b6aec 002_Ntr_BRCA_TCGA-BH-A0B5-11A_f478930d-216a-40ec-b434-bfc3a7b2f62b 002_Tex_BRCA_TCGA-BH-A0B5-01A_803de3d6-895f-4ad1-a86c-6f72d6ea8430 002_Ttr_BRCA_TCGA-BH-A0B5-01A_37175dfe-c34e-4f97-88b1-c0ba4bd5d093	0.7539	0.5	0.8944	0.575	0.6566
3	003_Nex_BRCA_TCGA-BH-A0BJ-11A_a9988fbb-090a-4363-bf73-7505e1710623 003_Ntr_BRCA_TCGA-BH-A0BJ-11A_2ced85bc-852a-4056-ad11-2e88ec6d2d82 003_Tex_BRCA_TCGA-BH-A0BJ-01A_58ec1111-c932-49ea-9327-1c64dfc2afa6 003_Ttr_BRCA_TCGA-BH-A0BJ-01A_73442f2d-3453-42ee-b57a-86871e2e2fd9	0.7386	0.37	0.8453	0.7	0.7458
4	004_Nex_BRCA_TCGA-E2-A158-11A_58fe3067-8198-486e-b0b2-286dc4451c39 004_Ntr_BRCA_TCGA-E2-A158-11A_323eb80d-71e2-4223-b471-a83ee42e6e08 004_Tex_BRCA_TCGA-E2-A158-01A_0329fa7e-d768-4bbe-940e-36f0b9829d7c 004_Ttr_BRCA_TCGA-E2-A158-01A_9d31f395-85e7-4ad8-95a3-0cc796c4b81d	0.9534	NaN	NaN	0.8	0.7799
5	005_Nex_BRCA_TCGA-A7-A13E-11A_bd7e6f8f-7213-4ded-a8ca-3c73c7b8d918 005_Ntr_BRCA_TCGA-A7-A13E-11A_99c08ce4-6526-4982-9bc7-b9c07972bcd5 005_Tex_BRCA_TCGA-A7-A13E-01A_28b8b84b-ca69-4c6a-860c-989777b18d32 005_Ttr_BRCA_TCGA-A7-A13E-01A_148d5aec-6026-46b5-b40c-38a1198175ab	0.909	0.83	0.9772	0.85	0.9184
6	006_Nex_BRCA_TCGA-BH-A208-11A_645b786f-1942-4cce-973b-4a75956265f5 006_Ntr_BRCA_TCGA-BH-A208-11A_a6dd96f4-f194-4c8d-8757-9e8b35465a9f 006_Tex_BRCA_TCGA-BH-A208-01A_5bdbc7db-ced4-4446-9069-c44c9c1f0ae0 006_Ttr_BRCA_TCGA-BH-A208-01A_794bcf95-8e66-4f91-a49c-ab10defc73c5	0.5951	0.31	0.6877	0.6	0.5642
7	007_Nex_BRCA_TCGA-BH-A1FU-11A_db7e821b-a2b6-40e1-9fbc-c72231b703a4 007_Ntr_BRCA_TCGA-BH-A1FU-11A_c051b92b-8e11-4623-b11b-3a0d52710663 007_Tex_BRCA_TCGA-BH-A1FU-01A_cb37bb7f-8f6b-432a-a58a-f8178d5baa64 007_Ttr_BRCA_TCGA-BH-A1FU-01A_7ea95c3a-b1a6-4658-b4c2-f35f3f48394e	0.6835	0.25	0.667	0.6	0.6121
8	008_Nex_BRCA_TCGA-BH-A0AY-11A_2ecc0325-3973-48b3-b53b-bb52aea5a9bc 008_Ntr_BRCA_TCGA-BH-A0AY-11A_1b2877ac-94a0-464c-b58b-9ce2f16aff37 008_Tex_BRCA_TCGA-BH-A0AY-01A_357ccb95-03e5-49f6-ab18-38d4c8d4d820 008_Ttr_BRCA_TCGA-BH-A0AY-01A_a19a60e7-e5ca-4f66-96fe-c9add702177d	0.6376	0.42	NaN	0.7	0.5612
9	009_Nex_BRCA_TCGA-BH-A18U-11A_bf3d62cb-f3a6-45d6-b9c3-416e58f1d319 009_Ntr_BRCA_TCGA-BH-A18U-11A_9d4c1d7e-dd77-41d1-b1df-144e7afb2141 009_Tex_BRCA_TCGA-BH-A18U-01A_a80933e5-3b07-41dc-b7f0-499d63c071a9 009_Ttr_BRCA_TCGA-BH-A18U-01A_ff89e0d9-7e6c-4b6b-a1c3-f800aaa414a1	0.7949	0.68	NaN	0.75	0.8077
10	010_Nex_BRCA_TCGA-AC-A2FF-11A_714e11fb-be71-4bbd-9327-457883a07ef0 010_Ntr_BRCA_TCGA-AC-A2FF-11A_4d32c4fa-959e-41cf-b837-104290bab9fa 010_Tex_BRCA_TCGA-AC-A2FF-01A_5c6fe1fc-839c-422a-89e7-4a54dcfad6c2 010_Ttr_BRCA_TCGA-AC-A2FF-01A_37bf962c-b180-4cc2-8e0b-fde78b4f99f4	0.5705	NaN	0.6868	0.8	0.6667
11	011_Nex_BRCA_TCGA-BH-A0BQ-11A_a5bdd116-8c1b-4787-be01-4c0f96709cc5 011_Ntr_BRCA_TCGA-BH-A0BQ-11A_45e17d22-fbed-418b-97fc-7104e1deac1 011_Tex_BRCA_TCGA-BH-A0BQ-01A_27138381-1865-4a6a-bd70-58725c92cb49 011_Ttr_BRCA_TCGA-BH-A0BQ-01A_8879454d-b803-40b6-b3d7-fbc295de9df6	0.6814	0.4	NaN	0.5	0.5779
12	012_Nex_BRCA_TCGA-BH-A0BA-11A_9dbc7f19-30bd-48fd-8d5a-ca67dc26c5b1 012_Ntr_BRCA_TCGA-BH-A0BA-11A_2cc17895-0a6e-4703-8164-7034f5c2e1a8 012_Tex_BRCA_TCGA-BH-A0BA-01A_b4c0df66-54c1-4bbf-9a3c-d2fd28d5bb4b 012_Ttr_BRCA_TCGA-BH-A0BA-01A_a9f9701c-6b4b-48ed-af83-94804fb098a8	0.7944	0.48	0.8945	0.87	0.7278
13	013_Nex_BRCA_TCGA-BH-A0B8-11A_ef67ace2-01d6-4e8b-92c7-7c4e1e5ca327 013_Ntr_BRCA_TCGA-BH-A0B8-11A_3a833d6d-75c7-4381-8cef-699c633b64e6 013_Tex_BRCA_TCGA-BH-A0B8-01A_54972439-f9da-497d-a605-24e9670021ad 013_Ttr_BRCA_TCGA-BH-A0B8-01A_9c7776d0-33df-4bd7-a720-807c650fdbc5	0.8571	0.87	0.9827	0.85	0.9342
14	014_Nex_BRCA_TCGA-BH-A0AU-11A_15483d36-ad24-4771-a991-8a8435effc6a 014_Ntr_BRCA_TCGA-BH-A0AU-11A_7f667d91-04aa-48e8-b675-9d99b64b2058 014_Tex_BRCA_TCGA-BH-A0AU-01A_e7a641f3-cc31-4319-a04b-75c42e991711 014_Ttr_BRCA_TCGA-BH-A0AU-01A_23e09239-bfc3-4c2e-b690-db940d5292f7	0.765	0.46	0.8525	0.775	0.652
15	015_Nex_BRCA_TCGA-BH-A18S-11A_9e6d6a2d-ce9e-4d44-9603-f843ffa06c63 015_Ntr_BRCA_TCGA-BH-A18S-11A_b54a0f88-21be-4c6d-a27a-1c1b8959652c 015_Tex_BRCA_TCGA-BH-A18S-01A_d4746397-9268-460a-954b-e5b5921138f9 015_Ttr_BRCA_TCGA-BH-A18S-01A_e0a3ea3a-ffce-4e30-9f42-cb047a7644a1	0.8948	0.89	NaN	0.85	0.8676

16	016_Nex_BRCA_TCGA-BH-A0HK-11A_d256dce0-d74b-4f8f-bf47-40b1b953fc7f 016_Ntr_BRCA_TCGA-BH-A0HK-11A_438650e8-0ee2-4c74-8432-88b5c8006187 016_Tex_BRCA_TCGA-BH-A0HK-01A_944b4c29-bf72-4eec-b277-badc237730de 016_Ttr_BRCA_TCGA-BH-A0HK-01A_fe04f368-0a73-4f97-9d6b-2986f9b2b052	0.7649	0.78	0.9163	0.925	0.8357
17	017_Nex_BRCA_TCGA-A7-A0D9-11A_dda70534-0d4d-4c30-9c6a-fb3c39396fb0 017_Ntr_BRCA_TCGA-A7-A0D9-11A_17cf6364-e228-4ee9-bffa-d1ad75f4152b 017_Tex_BRCA_TCGA-A7-A0D9-01A_821d7a33-77fb-496e-be9c-0552b12cbbec 017_Ttr_BRCA_TCGA-A7-A0D9-01A_c0ecd314-9d99-48ec-83f1-5a0c1ed656aa	0.8911	0.8	1	0.775	0.8921
18	018_Nex_BRCA_TCGA-BH-A0BV-11A_56dfc492-2b1f-4494-9ba9-14a70601ae21 018_Ntr_BRCA_TCGA-BH-A0BV-11A_20459115-d7bc-4d04-896f-c5ff6923ec4c 018_Tex_BRCA_TCGA-BH-A0BV-01A_beb9e4cf-1f76-4a26-acee-e88d0936e60b 018_Ttr_BRCA_TCGA-BH-A0BV-01A_d037d3c2-e316-473d-9970-d4fb43615d95	0.6895	0.54	NaN	0.725	0.6749
19	019_Nex_BRCA_TCGA-E2-A1LH-11A_61558dd3-8f6c-4f70-8717-7676580fa5a7 019_Ntr_BRCA_TCGA-E2-A1LH-11A_c7e02b93-465f-47da-81d7-ec9a8cb1e52b 019_Tex_BRCA_TCGA-E2-A1LH-01A_f54770bb-5dd0-48cf-ac5a-3f023a6aef95 019_Ttr_BRCA_TCGA-E2-A1LH-01A_169c390c-a211-4db0-a983-9bf5d6ee16e	0.5948	0.32	0.5637	0.8	0.4633
20	020_Nex_BRCA_TCGA-BH-A0DD-11A_e9fe9b97-f7c7-40dc-ae31-17bb15c9fd8b 020_Ntr_BRCA_TCGA-BH-A0DD-11A_5482cdd0-3698-455b-97c1-b10c69d67ae9 020_Tex_BRCA_TCGA-BH-A0DD-01A_99ca9706-f2bf-430b-9b23-e0947c0f8593 020_Ttr_BRCA_TCGA-BH-A0DD-01A_90cbc532-1ca8-46d6-977c-72b6d01e9c34	0.8677	0.79	0.9459	0.625	0.8714
21	021_Nex_BRCA_TCGA-BH-A0H5-11A_adfb1a86-fbb1-4b71-9c04-f99399f20d70 021_Ntr_BRCA_TCGA-BH-A0H5-11A_896d76a1-bae8-495a-9e12-e82e16bd8b16 021_Tex_BRCA_TCGA-BH-A0H5-01A_6cc3c90e-c77c-4609-ada5-9b78c659dc34 021_Ttr_BRCA_TCGA-BH-A0H5-01A_778c9326-998d-4081-b148-0eede2b94e29	0.4399	NaN	NaN	0.475	0.1632
22	022_Nex_BRCA_TCGA-A7-A0DB-11A_91081819-79c8-4de6-bfdb-742df760c08b 022_Ntr_BRCA_TCGA-A7-A0DB-11A_a8ed2ec3-0285-4028-9698-710a148ce11b 022_Tex_BRCA_TCGA-A7-A0DB-01A_37a9daca-9d53-4ec4-8de2-dc2c140a5d8f 022_Ttr_BRCA_TCGA-A7-A0DB-01A_1f62e969-d05d-4a4d-a163-cb06e4958f71	0.7341	0.44	NaN	0.85	0.6494
23	023_Nex_BRCA_TCGA-BH-A1FN-11A_e1c0d95f-949c-4cec-9cf8-f91c3b90b8d9 023_Ntr_BRCA_TCGA-BH-A1FN-11A_d5e5f3c9-4129-4c92-87f3-6f86577a7584 023_Tex_BRCA_TCGA-BH-A1FN-01A_8d715491-6943-4d58-92f6-88cce7b463e2 023_Ttr_BRCA_TCGA-BH-A1FN-01A_8e7dc738-8a8f-45b2-bd82-4125a07d7373	0.8367	0.7	0.8509	0.75	0.8313
24	024_Nex_BRCA_TCGA-BH-A0AZ-11A_9bbae9a0-9f12-48cf-9aa7-d070c6627ea5 024_Ntr_BRCA_TCGA-BH-A0AZ-11A_693bf8e4-b266-4b58-b812-f579179efb65 024_Tex_BRCA_TCGA-BH-A0AZ-01A_664528b7-b511-4627-8464-0702263434c5 024_Ttr_BRCA_TCGA-BH-A0AZ-01A_07f377f4-0bd1-4647-bf06-ff6ed553c44a	0.6505	0.53	0.8696	0.7	0.6655
25	025_Nex_BRCA_TCGA-BH-A0HA-11A_c61bb1ab-688f-4d58-8388-60ae77c28840 025_Ntr_BRCA_TCGA-BH-A0HA-11A_09e07a68-a443-4c16-a0de-78cd8aea59c0 025_Tex_BRCA_TCGA-BH-A0HA-01A_2c144eba-6490-4d64-9446-085d6edc8308 025_Ttr_BRCA_TCGA-BH-A0HA-01A_6d483def-2d91-4afc-991a-4a29804a6f3a	0.6418	0.74	0.9258	0.725	0.7386
26	026_Nex_BRCA_TCGA-A7-A0CE-11A_eee8d4d0-d524-47f5-b076-6ad6216de1a3 026_Ntr_BRCA_TCGA-A7-A0CE-11A_548cad87-ec95-47e2-890e-7c8284ea5b88 026_Tex_BRCA_TCGA-A7-A0CE-01A_4288da4e-7e77-434b-a092-9450b0cb7833 026_Ttr_BRCA_TCGA-A7-A0CE-01A_14201682-0c8d-49c7-a5e1-70261a07b69	0.9035	0.73	NaN	0.835	0.8551
27	027_Nex_BRCA_TCGA-BH-A0DK-11A_3f4400a1-84ab-4198-b9a1-67b2ffc5ef36 027_Ntr_BRCA_TCGA-BH-A0DK-11A_ae67044f-62c9-405f-bfc1-f0b8f1bc66d3 027_Tex_BRCA_TCGA-BH-A0DK-01A_e3e2053a-3ca2-4527-9b94-209def68dcc3 027_Ttr_BRCA_TCGA-BH-A0DK-01A_a3df35ec-a8d2-44ad-8ba6-eaba504261e0	0.5384	0.53	0.7316	0.7	0.6837
28	028_Nex_BRCA_TCGA-BH-A0E1-11A_f6fed4ed-a853-40aa-bf7b-e627efd402d6 028_Ntr_BRCA_TCGA-BH-A0E1-11A_52441de4-e26b-42b3-b061-94907c049501 028_Tex_BRCA_TCGA-BH-A0E1-01A_3c7e6a59-08b8-4903-932a-99946a96b746 028_Ttr_BRCA_TCGA-BH-A0E1-01A_f412f8d8-9e35-41d9-b44a-131186cb4bb0	0.8676	0.75	0.9742	0.825	0.8524
29	029_Nex_BRCA_TCGA-BH-A0DG-11A_c99b1fb3-17e3-4472-86ee-7fda358a92c2 029_Ntr_BRCA_TCGA-BH-A0DG-11A_bfdaf242-1e97-450d-9983-2cbb4e99305d 029_Tex_BRCA_TCGA-BH-A0DG-01A_721e2f71-60ae-4d63-9f05-113bce56c672 029_Ttr_BRCA_TCGA-BH-A0DG-01A_865afd6b-84a7-4dde-aa23-0b925c0b9d50	0.6358	0.42	0.7804	0.775	0.5386
30	030_Nex_BRCA_TCGA-AC-A2FB-11A_552279ea-d7b1-496d-8170-ca30f5b62b5a 030_Ntr_BRCA_TCGA-AC-A2FB-11A_56cd7da0-2c47-4986-91ce-07db2bb87369 030_Tex_BRCA_TCGA-AC-A2FB-01A_de000c35-8bf4-470a-9656-1b5da0deebef 030_Ttr_BRCA_TCGA-AC-A2FB-01A_35aa5078-e07f-4a0f-84c1-01a0e566e97c	0.5372	0.23	0.5493	0.7	0.4436
31	031_Nex_BRCA_TCGA-BH-A0H7-11A_abfca562-d328-40d2-83bb-e584123b0f28 031_Ntr_BRCA_TCGA-BH-A0H7-11A_d969d9b2-9d8b-4594-95d4-87e6ce1236fc 031_Tex_BRCA_TCGA-BH-A0H7-01A_e8daad78-39fc-4835-b1c4-8807653d9c9a	0.7939	0.63	0.9561	0.725	0.7534

	031_Ttr_BRCA_TCGA-BH-A0H7-01A_0d37f87a-760a-472a-acba-bbc255422fbc					
32	032_Nex_BRCA_TCGA-BH-A1EU-11A_38e87966-9605-4454-a4d1-28f96b7689f7 032_Ntr_BRCA_TCGA-BH-A1EU-11A_3b00c121-17f2-461e-8873-08d15c9ec9f4 032_Tex_BRCA_TCGA-BH-A1EU-01A_4bccbb0f-2641-44df-b89a-42f020b4c08f 032_Ttr_BRCA_TCGA-BH-A1EU-01A_86e3dba1-48fb-44cc-b046-8bc35963ce99	0.5387	0.33	0.6869	0.65	0.4299
33	033_Nex_BRCA_TCGA-BH-A0DP-11A_27543260-52ac-444b-8214-e62dca2cc8fe 033_Ntr_BRCA_TCGA-BH-A0DP-11A_30f4e5d8-a13d-4ef2-88e0-a01e07c2e142 033_Tex_BRCA_TCGA-BH-A0DP-01A_0326975a-2e56-404a-8776-92c5c5678853 033_Ttr_BRCA_TCGA-BH-A0DP-01A_7ff8a7a0-5235-4de0-bb9f-b811230b5bda	0.7037	0.42	0.8565	0.7	0.655
34	034_Nex_BRCA_TCGA-BH-A18N-11A_6c8aae77-5f43-41ec-a139-81f3ba02f6ea 034_Ntr_BRCA_TCGA-BH-A18N-11A_0738f1b2-aa50-4921-82e1-d3614b40f98d 034_Tex_BRCA_TCGA-BH-A18N-01A_b6f89799-9070-4fbc-b10c-53cbe515eccc 034_Ttr_BRCA_TCGA-BH-A18N-01A_4b7b8eb8-d939-411c-be5e-cf41a5521963	0.8685	0.76	NaN	0.9	0.832
35	035_Nex_BRCA_TCGA-BH-A0BC-11A_6359db46-f8dd-4dc8-a3a9-8725d8f6958a 035_Ntr_BRCA_TCGA-BH-A0BC-11A_2cb50d4a-d6df-4b64-acfb-7a7db5ddd1de 035_Tex_BRCA_TCGA-BH-A0BC-01A_73b9208d-336c-4990-a27d-0164a77dd165 035_Ttr_BRCA_TCGA-BH-A0BC-01A_92e26b53-f540-428a-a3c5-848a36b31171	0.6221	0.6	0.8221	0.8	0.7727
36	036_Nex_BRCA_TCGA-BH-A0BZ-11A_2b4e3d99-07cd-4b06-ad97-82a19ac0eb5d 036_Ntr_BRCA_TCGA-BH-A0BZ-11A_3aa16a4b-4e35-4530-84fb-0cb204290b08 036_Tex_BRCA_TCGA-BH-A0BZ-01A_74414845-839f-4885-b13d-3f2e17781f84 036_Ttr_BRCA_TCGA-BH-A0BZ-01A_efefcc2f-72e9-4634-b943-d26083e1a312	0.5788	0.37	0.7363	0.6	0.5138
37	037_Nex_BRCA_TCGA-BH-A0DL-11A_2d495f9c-4ffa-4169-b583-6786612e9606 037_Ntr_BRCA_TCGA-BH-A0DL-11A_bd8b100a-8391-4046-847f-c3fdd3830eeb 037_Tex_BRCA_TCGA-BH-A0DL-01A_dfd355e4-478a-47cb-9aab-8ce22b6f936c 037_Ttr_BRCA_TCGA-BH-A0DL-01A_11d77ef2-b3f9-4af9-8490-71f9a8c599e0	0.6944	0.53	NaN	0.65	0.6655
38	038_Nex_BRCA_TCGA-BH-A0BT-11A_32430467-5215-4738-86a3-5bbe11fbba86 038_Ntr_BRCA_TCGA-BH-A0BT-11A_cbef4196-5f3b-40d9-b26f-5b2bb82fbc9b 038_Tex_BRCA_TCGA-BH-A0BT-01A_e78b9962-7bc2-4238-806a-5933ac07de99 038_Ttr_BRCA_TCGA-BH-A0BT-01A_aae75165-efa0-46b3-8a8d-82dc7d82aecd	0.8096	0.67	0.9054	0.75	0.7751
39	039_Nex_BRCA_TCGA-BH-A18Q-11A_b58d4f69-a4ea-489b-9d25-e5cfdc465adb 039_Ntr_BRCA_TCGA-BH-A18Q-11A_76575097-374b-4fb2-8054-2a31b4204165 039_Tex_BRCA_TCGA-BH-A18Q-01A_1f2c90ef-a05d-494c-9232-e705691f46b9 039_Ttr_BRCA_TCGA-BH-A18Q-01A_f0173e28-7fe4-411f-a187-57fd94a7935a	0.8117	0.73	NaN	0.9	0.836
40	040_Nex_BRCA_TCGA-E2-A1LB-11A_e2d7a695-b0bf-4432-8f98-1843bb49efba 040_Ntr_BRCA_TCGA-E2-A1LB-11A_6eb518ab-f174-45ae-8d65-74086ecb1125 040_Tex_BRCA_TCGA-E2-A1LB-01A_3ddbc444-ee1b-43be-bab5-b0f67d5eb339 040_Ttr_BRCA_TCGA-E2-A1LB-01A_d7d566a0-b6d0-4a4f-8211-9309b27b0ade	0.8415	0.68	0.8192	0.9	0.815
41	041_Nex_BRCA_TCGA-BH-A0DH-11A_a7a7e0f6-100f-4145-9599-693e6c14e903 041_Ntr_BRCA_TCGA-BH-A0DH-11A_5a0374e5-ccc9-4952-9df0-4ff125196478 041_Tex_BRCA_TCGA-BH-A0DH-01A_eb680f8c-4ba1-45ef-8b94-e58b68922f2f 041_Ttr_BRCA_TCGA-BH-A0DH-01A_71a3c27c-0982-4da6-b260-cf16a4868a19	0.8317	0.76	0.8955	0.85	0.8597
42	042_Nex_BRCA_TCGA-BH-A0B7-11A_d9aca915-ea30-4939-af59-edaef8872396 042_Ntr_BRCA_TCGA-BH-A0B7-11A_8db8b247-05b8-46ca-8791-ecf846da2c7f 042_Tex_BRCA_TCGA-BH-A0B7-01A_e3b9eb8a-93f3-4668-a54b-fa8b15be5667 042_Ttr_BRCA_TCGA-BH-A0B7-01A_0fdae4ee-ca68-4ba4-ba58-76058409b02f	0.6207	0.2	NaN	0.575	0.4954
43	043_Nex_BRCA_TCGA-E2-A15I-11A_36024763-f828-4496-8fdc-46d5c3de569b 043_Ntr_BRCA_TCGA-E2-A15I-11A_ffa9ace8-9253-4775-9ad2-2a8a50c0f9c9 043_Tex_BRCA_TCGA-E2-A15I-01A_8c627466-eb99-4a7e-87e6-314ac8ed32a1 043_Ttr_BRCA_TCGA-E2-A15I-01A_3a4e3785-fb2e-4ffc-9644-91c78a9a9ebe	0.7689	0.62	0.768	0.8	0.7565
44	044_Nex_BRCA_TCGA-BH-A0DV-11A_79a92eab-c87c-4209-819e-193d653c0df6 044_Ntr_BRCA_TCGA-BH-A0DV-11A_e87e7e3e-9059-47cf-9f45-8959250b037f 044_Tex_BRCA_TCGA-BH-A0DV-01A_105290eb-b626-4318-9b8a-42f477e2cec6 044_Ttr_BRCA_TCGA-BH-A0DV-01A_7bad3f4c-6065-4245-8119-c25596f38829	0.6021	0.31	0.7631	0.7	0.4856
45	045_Nex_BRCA_TCGA-BH-A0DZ-11A_aebf0d4d-4a1b-4a50-b5f1-0f9e2c273121 045_Ntr_BRCA_TCGA-BH-A0DZ-11A_80b4d43d-9e7d-4ab8-b05a-0eb51faa9d12 045_Tex_BRCA_TCGA-BH-A0DZ-01A_4e7d62f5-4be9-4b9c-9b7c-aec4567dded2 045_Ttr_BRCA_TCGA-BH-A0DZ-01A_8b1982a0-315c-47e1-8de0-a1e5ec51dd74	0.6572	0.65	NaN	0.885	0.7792
46	046_Nex_BRCA_TCGA-BH-A18R-11A_b32b2067-a79e-42c5-ae78-135c845253fe 046_Ntr_BRCA_TCGA-BH-A18R-11A_f82099ae-9d74-44d8-ba5b-cd10eeb09807 046_Tex_BRCA_TCGA-BH-A18R-01A_c518bc34-50dc-4265-824f-a954e4d19f0b 046_Ttr_BRCA_TCGA-BH-A18R-01A_fc65ff2e-9808-4c1e-a16b-8285fd0d27df	0.8685	0.53	NaN	0.85	0.7466
47	047_Nex_BRCA_TCGA-E2-A15K-11A_6299f114-932a-42c0-8cab-bebb12c996fc	0.7425	0.7	0.724	0.9	NaN

	047_Ntr_BRCA_TCGA-E2-A15K-11A_c2ab9488-d9a4-479c-b9e2-6f9b0cdbaacb					
	047_Tex_BRCA_TCGA-E2-A15K-01A_80019ec7-b0d8-4573-b5d6-a5d9f2745ab2					
	047_Ttr_BRCA_TCGA-E2-A15K-01A_7e3a600b-edd8-428e-b88d-af4c63dcaad9					
48	048_Nex_BRCA_TCGA-BH-A1EN-11A_a6259119-3d8a-4749-a517-c675efbc8215	0.8518	0.7	0.9612	0.85	0.8179
	048_Ntr_BRCA_TCGA-BH-A1EN-11A_488f1b69-c2a3-429b-a972-31edfd615a67					
	048_Tex_BRCA_TCGA-BH-A1EN-01A_72e4cb26-911c-4804-9e4f-ed5b51024cd1					
	048_Ttr_BRCA_TCGA-BH-A1EN-01A_96360e75-26b6-4647-b974-9e31ae6de00c					
49	049_Nex_BRCA_TCGA-BH-A0H9-11A_d8b452e5-010a-4fec-80a4-770a5a492090	0.8872	0.35	0.7934	0.7	0.747
	049_Ntr_BRCA_TCGA-BH-A0H9-11A_1337ceba-db77-4b31-ac20-1c6a8bb5f546					
	049_Tex_BRCA_TCGA-BH-A0H9-01A_ac4899fe-f56d-4b98-9a54-73ffd0c90652					
	049_Ttr_BRCA_TCGA-BH-A0H9-01A_a97d281f-235f-481b-b26b-169b96e0e65f					
50	050_Nex_BRCA_TCGA-E2-A153-11A_1c3f2e11-952a-4e47-a8b9-25f4fe4bf205	0.6589	0.61	NaN	0.6	0.5474
	050_Ntr_BRCA_TCGA-E2-A153-11A_bd0ab51c-c114-40e3-a6a1-4b8f576a41d3					
	050_Tex_BRCA_TCGA-E2-A153-01A_85258fb2-26ab-4a66-b8a5-5a58bf9275e0					
	050_Ttr_BRCA_TCGA-E2-A153-01A_091a54cd-c3b3-4af2-828f-a80e64504f5e					
51	051_Nex_BRCA_TCGA-BH-A0BW-11A_ab130f7f-4070-436e-ac7b-c1b7aecb9dc6	0.6784	0.54	NaN	0.6	0.6749
	051_Ntr_BRCA_TCGA-BH-A0BW-11A_2581c95b-1b57-4407-bbc4-a65c89bfd136					
	051_Tex_BRCA_TCGA-BH-A0BW-01A_7661179f-df6c-4a57-adca-224b62d98348					
	051_Ttr_BRCA_TCGA-BH-A0BW-01A_a15d171e-ac82-4712-94a9-b4799e7b2915					
52	052_Nex_BRCA_TCGA-BH-A18J-11A_3aa5b173-17b2-425f-b5c7-395614d6bfa2	0.8066	0.51	NaN	0.7	0.7243
	052_Ntr_BRCA_TCGA-BH-A18J-11A_307eb339-a781-45cc-9597-da0be7e5438a					
	052_Tex_BRCA_TCGA-BH-A18J-01A_f639a485-8ebb-4dcc-9f2e-a8d7ad05564f					
	052_Ttr_BRCA_TCGA-BH-A18J-01A_0e985713-0492-4191-918b-fef6c23389b1					
53	053_Nex_BRCA_TCGA-BH-A204-11A_98e5c1d8-5c14-4416-8437-31d0098dd341	0.8763	0.89	0.9364	0.85	0.9601
	053_Ntr_BRCA_TCGA-BH-A204-11A_2afdc0cf-2723-42dd-89f7-fa03c6ba218c					
	053_Tex_BRCA_TCGA-BH-A204-01A_970600ce-9486-4641-8555-533132f7a414					
	053_Ttr_BRCA_TCGA-BH-A204-01A_893fcf87-8baa-424e-8866-bcf8cfa26cf9					
54	054_Nex_BRCA_TCGA-BH-A18K-11A_502ee86f-829e-4b6e-a8f1-be082c445310	0.8058	0.58	NaN	0.8	0.7468
	054_Ntr_BRCA_TCGA-BH-A18K-11A_375bcd8d-8628-4047-948a-fa98bfa3dba5					
	054_Tex_BRCA_TCGA-BH-A18K-01A_7e8c2ea7-04ce-47c5-b848-229f96563015					
	054_Ttr_BRCA_TCGA-BH-A18K-01A_12473f59-359c-4306-ade3-2156e458cd05					
55	055_Nex_BRCA_TCGA-BH-A0C3-11A_9fedd2f4-d2c8-4d24-987b-69edf55e15f1	0.6289	0.39	0.7847	0.45	0.528
	055_Ntr_BRCA_TCGA-BH-A0C3-11A_a49fa48d-efc4-4b99-a42e-7019236af6c8					
	055_Tex_BRCA_TCGA-BH-A0C3-01A_866d9cb0-a299-46c1-a787-2e73fd758fbc					
	055_Ttr_BRCA_TCGA-BH-A0C3-01A_164f86df-dec9-44ef-b1c7-2ee5d33617be					
56	056_Nex_BRCA_TCGA-BH-A0C0-11A_9778035c-19ff-4a89-bba2-fa83e51d9add	0.6223	0.27	0.5586	0.85	0.5068
	056_Ntr_BRCA_TCGA-BH-A0C0-11A_52a72824-0b41-4b8e-86f0-41ee5e00c989					
	056_Tex_BRCA_TCGA-BH-A0C0-01A_568a2363-b7e5-48f6-9242-328950eebf39					
	056_Ttr_BRCA_TCGA-BH-A0C0-01A_f5fe9655-f5b4-413b-882c-43b872e4ec23					
57	057_Nex_BRCA_TCGA-BH-A0E0-11A_59fa57c8-7435-4499-bd09-bf969596c18d	0.9013	0.57	0.7391	0.875	0.7486
	057_Ntr_BRCA_TCGA-BH-A0E0-11A_a3e5f7bd-3ab0-4ea6-9de1-742de1a2ed78					
	057_Tex_BRCA_TCGA-BH-A0E0-01A_72436fcd-21fd-46bd-bd36-7f514edb51de					
	057_Ttr_BRCA_TCGA-BH-A0E0-01A_b98d2a16-974c-4728-9648-81dc4314f225					
58	058_Nex_BRCA_TCGA-BH-A18M-11A_8e0cb775-9fc9-4001-973c-ef6cec2a38b6	0.7363	0.45	NaN	0.85	0.6525
	058_Ntr_BRCA_TCGA-BH-A18M-11A_3e02aa37-30ee-4663-bba1-280e5127f302					
	058_Tex_BRCA_TCGA-BH-A18M-01A_69ccc418-264c-4e8e-a034-39607c07fa59					
	058_Ttr_BRCA_TCGA-BH-A18M-01A_aea8ff88-dbc9-4a1b-9a3a-ca1882432c57					
59	059_Nex_BRCA_TCGA-E2-A1BC-11A_45b8b995-c477-4358-8050-6d41c267b467	0.8083	0.56	0.8676	0.85	0.7707
	059_Ntr_BRCA_TCGA-E2-A1BC-11A_205007dd-4bc1-4e1f-9fdb-115b0e7c9836					
	059_Tex_BRCA_TCGA-E2-A1BC-01A_f969cce4-0fcd-47bb-91f1-37ba0f314994					
	059_Ttr_BRCA_TCGA-E2-A1BC-01A_ea3bd91d-520b-4198-b011-a0f578eadc3e					
60	060_Nex_BRCA_TCGA-BH-A203-11A_f08939ed-a218-4688-b419-a91333d0267b	0.7637	0.37	0.6872	0.75	0.5905
	060_Ntr_BRCA_TCGA-BH-A203-11A_8c2d82aa-0b36-488f-8cf1-f82795b831c5					
	060_Tex_BRCA_TCGA-BH-A203-01A_55a9b84d-ca9f-402c-8d93-15aef2fde988					
	060_Ttr_BRCA_TCGA-BH-A203-01A_8986bdd8-2be5-41ed-9596-59ca1f95e1c0					
61	061_Nex_BRCA_TCGA-BH-A1F2-11A_d6eb2d94-1234-46b3-9403-958f3b340fd0	0.7507	0.52	0.8661	0.6	0.754
	061_Ntr_BRCA_TCGA-BH-A1F2-11A_210014fa-f161-4799-a1c0-6f93d4b631f6					
	061_Tex_BRCA_TCGA-BH-A1F2-01A_91aeda5a-ed5a-4175-b19e-408219b980fc					
	061_Ttr_BRCA_TCGA-BH-A1F2-01A_ceb5a503-e107-4721-9283-714406cdd914					
62	062_Nex_BRCA_TCGA-BH-A1EO-11A_90308930-e3c5-47bb-bcee-58eae7d3dfa	0.5849	0.48	0.8854	0.9	0.7493
	062_Ntr_BRCA_TCGA-BH-A1EO-11A_a426d9c2-86b1-4db1-b49c-ecceaa01273a9					
	062_Tex_BRCA_TCGA-BH-A1EO-01A_7787e3e2-f604-4b4d-a3bc-60c795d4177b					
	062_Ttr_BRCA_TCGA-BH-A1EO-01A_e31bd4a4-ecda-49b4-83b0-7f1496c2f9ae					

63	063_Nex_BRCA_TCGA-BH-A18V-11A_353e7fa1-08c5-400a-b352-b5325e40d66c	0.6941	0.56	NaN	0.75	NaN
	063_Ntr_BRCA_TCGA-BH-A18V-11A_e3c5cba8-e3ba-4e0b-929b-280708e0a855					
	063_Tex_BRCA_TCGA-BH-A18V-01A_abcfa8e-6f4c-4668-9ef9-41d95d16e8e6					
	063_Ttr_BRCA_TCGA-BH-A18V-01A_286394db-7d5e-4de2-b386-581352164350					
64	064_Nex_BRCA_TCGA-BH-A0DT-11A_6dde640a-1d79-4e7d-9491-c500b8183d9a	0.7462	0.42	NaN	0.55	0.6659
	064_Ntr_BRCA_TCGA-BH-A0DT-11A_71aa4cd6-75ea-4e10-b16c-ea9adbf31a98					
	064_Tex_BRCA_TCGA-BH-A0DT-01A_9d93c6fb-336a-4cb4-9f33-8557456753b1					
	064_Ttr_BRCA_TCGA-BH-A0DT-01A_61ad7408-dacd-4913-a479-c456e8b03191					
65	065_Nex_BRCA_TCGA-GI-A2C9-11A_454dbdba-da53-4e99-9670-dff1e5bbb77c	0.8062	0.51	0.8386	0.8	0.6969
	065_Ntr_BRCA_TCGA-GI-A2C9-11A_d8aa0349-d74e-4891-8398-6476eb1935f0					
	065_Tex_BRCA_TCGA-GI-A2C9-01A_2f2b0909-488b-4fa3-8251-2ef6e7d5869e					
	065_Ttr_BRCA_TCGA-GI-A2C9-01A_01ea694e-989b-4a35-9397-5e508656d1d8					
66	066_Nex_BRCA_TCGA-BH-A209-11A_c580c610-832d-45be-9963-06bb918ede73	0.5979	0.24	0.6243	0.6	0.4645
	066_Ntr_BRCA_TCGA-BH-A209-11A_b8b48554-ca2f-466d-85b0-9d473cca8ca7					
	066_Tex_BRCA_TCGA-BH-A209-01A_7b85ca36-2fe9-4156-99eb-f79463dbc572					
	066_Ttr_BRCA_TCGA-BH-A209-01A_b2cf947a-5ed1-4e24-8752-bf2a6eca895a					
67	067_Nex_BRCA_TCGA-BH-A1EV-11A_f4d30842-7873-46d3-8f25-ac7d05909175	0.8435	0.61	0.9517	0.8	0.817
	067_Ntr_BRCA_TCGA-BH-A1EV-11A_73e296db-9eec-4060-97c9-80a98dbb9fb6					
	067_Tex_BRCA_TCGA-BH-A1EV-01A_fb502696-cb13-487a-a70a-6ceefcf20ca0					
	067_Ttr_BRCA_TCGA-BH-A1EV-01A_93ab3adf-7ab9-455e-9007-9f51443352fe					
68	068_Nex_BRCA_TCGA-GI-A2C8-11A_836e4482-11c7-4422-a2e5-cac9b846ea71	0.601	0.48	0.7846	0.85	0.6998
	068_Ntr_BRCA_TCGA-GI-A2C8-11A_580d9a3d-e198-4e7b-aa1f-419d868bb0b5					
	068_Tex_BRCA_TCGA-GI-A2C8-01A_146c0ba4-6761-446c-be7c-7e56c0ffa37b					
	068_Ttr_BRCA_TCGA-GI-A2C8-01A_c0ee6e25-02b9-4b2f-9f23-fd61eedf9945					
69	069_Nex_BRCA_TCGA-BH-A0BM-11A_92faafbd-6a76-4116-80fc-a15767aa81d0	0.796	0.61	0.9189	0.84	0.7886
	069_Ntr_BRCA_TCGA-BH-A0BM-11A_ac127be2-5e4c-4b7e-9cf8-3aa9e529baaa					
	069_Tex_BRCA_TCGA-BH-A0BM-01A_c513ed81-255f-43b0-b8aa-984326201745					
	069_Ttr_BRCA_TCGA-BH-A0BM-01A_006b2b95-7069-4cb6-bfe8-7edb80056add					
70	070_Nex_BRCA_TCGA-BH-A18L-11A_7a010ccd-f780-45f0-98da-cc738e87b6d3	0.927	0.81	NaN	0.8	0.9113
	070_Ntr_BRCA_TCGA-BH-A18L-11A_ef4660c0-c177-4d46-90f9-56e3dc47b59e					
	070_Tex_BRCA_TCGA-BH-A18L-01A_0d4aca9c-c11e-4f78-a250-08d45ce4828e					
	070_Ttr_BRCA_TCGA-BH-A18L-01A_1af43803-7afa-4d2b-aa78-2dec84c1e702					
71	071_Nex_BRCA_TCGA-A7-A13F-11A_471d1e10-7c79-44f9-a373-bd3e510b6155	0.8478	0.65	0.9236	0.7	0.7915
	071_Ntr_BRCA_TCGA-A7-A13F-11A_4e4cd9e5-27bb-4ea7-9328-0b267373ec1c					
	071_Tex_BRCA_TCGA-A7-A13F-01A_d8fad6b2-66b8-4d6f-b018-653998675921					
	071_Ttr_BRCA_TCGA-A7-A13F-01A_75898a6d-75e4-4dca-a7ed-c11056e0c9c4					
72	072_Nex_BRCA_TCGA-E2-A15M-11A_b2138cda-519f-4691-bf1c-0f863b55d888	0.4911	0.28	NaN	0.8	0.4285
	072_Ntr_BRCA_TCGA-E2-A15M-11A_bf873756-8ee8-49bd-b2ca-17223c7ef962					
	072_Tex_BRCA_TCGA-E2-A15M-01A_1ccf392d-7959-4bb9-8ca8-4298409f4951					
	072_Ttr_BRCA_TCGA-E2-A15M-01A_b2569032-6147-4a1c-973f-d5985127e9f4					